Scilight

Power Electronics Research and Applications Transactions

https://www.sciltp.com/journals/perat



Check for updates

Review

Condition Monitoring and Operation Optimization of Power Electronic Components and Systems

Huai Wang

Department of Energy, Aalborg University, 9220 Aalborg, Denmark; hwa@energy.aau.dk

How To Cite: Wang, H. Condition Monitoring and Operation Optimization of Power Electronic Components and Systems. *Power Electronics Research and Applications Transactions* **2026**. https://doi.org/10.53941/perat.2026.100015

Received: 28 September 2026
Revised: 8 October 2026
Accepted: 8 October 2026
Published: 13 October 2026

Abstract: This perspective paper examines the research gaps, methodological frameworks, and future directions for degradation estimation, fault pre-warning, and operation optimization of power electronic components and systems. Reliability and availability have become as decisive as efficiency and power density in many applications, because unplanned downtime, maintenance, and premature end of life contribute substantially to the life-cycle cost of ownership. Despite extensive academic research on condition monitoring of DC-link capacitors and power semiconductor devices, on prognostics, and on reliability-oriented control, a gap persists between the reported advances and the needs and constraints of industrial deployment. Drawing on a review of these developments, the paper identifies the scientific and implementation challenges involved and discusses methodological perspectives that connect failure time scales, monitoring implementation, end-of-life criteria, performance verification, and operation optimization across component and system levels, covering model-based, data-driven, and hybrid approaches. Finally, it outlines research directions toward more reliable, highly available, and cost-effective power electronic systems through condition-aware and risk-informed operation.

Keywords: condition monitoring; DC-link capacitors; end of life; failure time scales; fault pre-warning; operation optimization; power semiconductor devices; prognostics and health management (PHM); remaining useful life (RUL); verification

1. Introduction

Power electronic converters are on the critical path of electric vehicles (EVs), rail traction, aircraft, renewable generation, and data centers, and a converter failure can stop the whole service. Reliability and availability have become design targets on a par with efficiency and power density. The European Center for Power Electronics (ECPE) surveyed its member companies on the trends expected to improve future reliability [1]. Condition monitoring (CM) and control that avoids stressful operating conditions received the second-highest scores, after the use of components proven to be robust and reliable [1]. Only 13 % of the 51 respondents considered the current quantity and focus of reliability research adequate [1]. An earlier industry survey identified a significant need for better reliability-monitoring methods and indicators [2]. Field studies show why this need persists. In wind-turbine converters, thermal-cycling fatigue of bond contacts and die-attach solder is not a relevant cause of the observed failures, whereas humidity is a likely driver [3,4]. Basic tests or electrical characteristics may not reveal the health state of insulated-gate bipolar transistors IGBTs after a fault or after years of service [5,6].

The underlying techniques have been reviewed extensively, but mostly by physical principle rather than by the conditions that decide deployment. Reviews cover CM for device reliability [7,8] and the reliability and CM of DC-link capacitors [9–11], the latter classified by measurement principle and by online or offline use. Further reviews address the physics of failure and prognostics of IGBT modules [12], junction-temperature measurement with temperature-sensitive electrical parameters (TSEPs) [13,14], artificial intelligence (AI) for power electronics [15],



Copyright: © 2026 by the authors. This is an open access article under the terms and conditions of the Creative Commons Attribution (CC BY) license (https://creativecommons.org/licenses/by/4.0/).
Publisher's Note: Scilight stays neutral with regard to jurisdictional claims in published maps and institutional affiliations.

the cost and complexity of intelligent maintenance [16], and the state of the art of power electronics reliability [17]. IEEE Std 1856-2017 defines a framework for prognostics and health management (PHM) of electronic systems, and ISO 13381-1 gives general guidelines for the prognostics of machines [18,19]. These publications remain the reference for individual health indicators, measurement circuits, and algorithms, and they are not repeated here.

The existing reviews rarely address why so few of the reported methods have been adopted in industrial applications. The contribution of this paper lies in new perspectives on condition monitoring and operation optimization, with the following specific aspects: (1) a systematic mapping of failure and degradation mechanisms, their time scales, and the resulting opportunities for protection, fault diagnosis, and prognosis; (2) a summary of the operation windows available for condition monitoring of long-term degradation and for the estimation of the remaining useful life (RUL); (3) an update, from the implementation perspective, of the classification of condition monitoring methods used in most of the existing literature; (4) a more comprehensive set of end-of-life (EOL) criteria; (5) an analysis of the limitations of the existing verification methods; and (6) a placement of the measures of operation optimization, with their side effects, on the same time axis as the failure processes. Based on these perspectives, six future research directions are discussed.

2. Failure and Degradation Processes on a Time-Scale Axis

The classification of a failure as catastrophic or wear-out describes its end state. Whether the failure can be managed depends on the time between the first detectable change and the loss of function, which reliability-centered maintenance calls the P–F interval [20]. Let T_W denote this warning window, T_D the detection latency of a monitoring function, and T_A the time needed to act, all in seconds. The action may be to turn off a device, to derate, or to schedule a service visit. The function is feasible only if $T_D + T_A < T_W$. The condition applies to protection, diagnostics, and prognostics alike. For events without a precursor, T_W is essentially zero, and only a reactive protection or a design margin remains. For power electronic components, the warning windows of the processes in Figure 1 span about 18 orders of magnitude, from below a nanosecond to about 20 years.

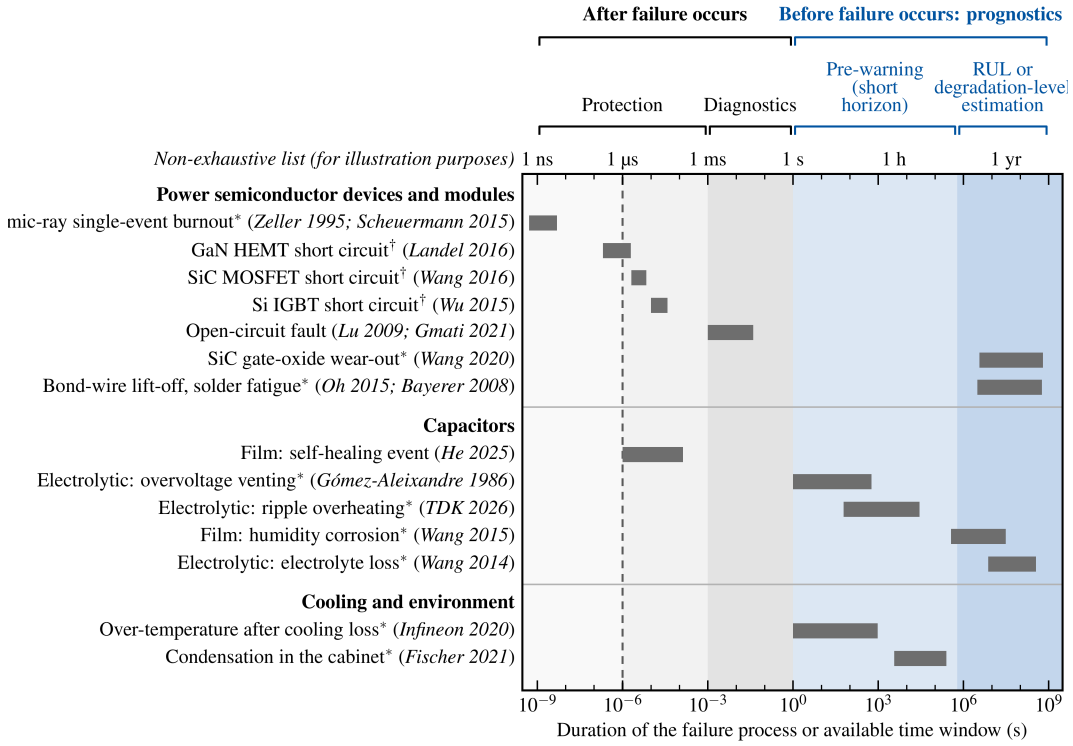


Figure 1. Failure and degradation processes of power electronic components and systems on a logarithmic time axis (non-exhaustive, for illustration). The axis is divided into actions after a failure occurs (protection and diagnostics, gray) and before it occurs (prognostics, blue). The prognostics band is split into short-horizon pre-warning and long-horizon estimation of the RUL or degradation level. Each bar shows the time scale of the failure process, i.e., the window T_W available for the actions at the top. Band boundaries are indicative. The dashed line at 1 µs marks the range in which protection overlaps with device and gate-driver design. * Duration estimated. † Indicative durations. The cited references address the short-circuit capability of the respective devices, not these exact ranges. Studies cited in the figure: refs. [4,9,12,21–34].

Figure 1 is divided into four functional bands. Each bar shows the time scale of the failure process, which is also the window T_W available for the actions at the top of the figure. A function in a band is feasible only if its T_D + T_A is shorter than the bars in that band. Protection covers nanoseconds to about a millisecond, including short circuits of IGBTs, SiC metal–oxide–semiconductor field-effect transistors (MOSFETs), and GaN high-electron-mobility transistors (HEMTs) [21–23] and cosmic-ray-induced burnout, which has no measurable precursor [24,25]. The band boundaries depend on the device technology. At high DC-link voltage and temperature, commercial SiC MOSFETs withstand a short circuit for only several microseconds [22], and GaN HEMTs can fail after only a few hundred nanoseconds, although their robustness is widely dispersed [23]. For both, short-circuit protection becomes part of the gate-driver design. Protection, device design, and monitoring overlap here. Diagnostics covers milliseconds to seconds, mainly open-circuit faults, which established methods diagnose within a fraction of a fundamental period to about two periods [26,27]. Pre-warning covers seconds to about a week: over-temperature after a loss of cooling, overvoltage and ripple overload of electrolytic capacitors, and condensation [4,28–30]. Partial discharge in power-module packaging under the fast voltage transitions of wide-bandgap devices is a further precursor. In the long run, it can degrade the silicone gel and the substrate and eventually lead to breakdown [35]. Measurable precursors exist for these processes, yet measured distributions of the lead time between precursor and failure are absent from the literature reviewed for this paper. Long-horizon prognostics covers weeks to years: gate-oxide wear-out, humidity-driven corrosion of film capacitors, electrolyte loss, and bond-wire and solder fatigue [9,12,31–33]. Most CM studies address this band.

The time axis has three consequences. The sampling and decision rate of a monitoring function should be derived from T_W of the fastest failure mode it is meant to cover. Fast events can also provide data for long-horizon prognostics. A self-healing event of a film capacitor lasts microseconds, and its energy and duration relate to the damage of the electrode and the film and thus to the loss of capacitance [34]. The pre-warning band has received the least attention in condition monitoring research, although its precursors are known. It is a promising field for research. The remainder of this paper uses long-horizon degradation estimation and RUL prognostics as the running example.

3. Classification of Condition Monitoring Methods

This section separates the two attributes of a monitoring method that decide its deployability, reviews the operation windows in which health indicators can be acquired, proposes a classification on these two attributes, and illustrates the classification with four examples.

3.1. Hardware Implementation and Processing

The conventional classes (sensor-based, model-based, and data-driven) [10] conflate two attributes. A monitoring function first obtains health indicators typically from currents, voltages, and temperatures, which determines its hardware implementation and hence its cost, risk, and certification effort for the product. It then processes the health indicators, or the measured signals directly, into information for diagnostics, prognostics, and actions, which can be model-based, data-driven, or hybrid. The first attribute largely decides whether a method can be deployed, and the second how well it infers the health state. Recent work already emphasizes the first attribute, for instance by estimating the capacitance without hardware or software modification [36] or by limiting the additional risk that monitoring introduces [37]. In practice, several models are often combined to make the prediction more robust [38].

3.2. Operation Modes and Service Life

Most methods are designed for normal operation, where load dynamics, switching noise, and the risk of interfering with the operation are largest. Special operation modes offer more favorable conditions and occur frequently (Figure 2a). Household vehicles in the United States are parked for about 95 % of a typical day and driven for 64.6 min on average (2022 data) [39]. Each shutdown of an EV traction inverter includes an active DC-link discharge. Post-crash safety regulations accept, among alternative criteria, a high-voltage bus voltage of at most 60 V DC, measured from 5 s after the impact [40,41]. After a regular shutdown, the discharge has to comply with regulatory limits, for example, less than 5 s in the European Union and less than 3 s in China [42]. Railway traction converters undergo a nighttime routine inspection [43], and aircraft drives perform a discharge after each landing [44]. The windows depend on the operating strategy: a photovoltaic (PV) inverter that provides reactive power at night, for example, has no idle window and has to rely on online methods (rows C and D of the classification in Section 3.3). Such windows have been used mainly for capacitor monitoring [45–48] and less often for semiconductors [49,50], and continuously operating systems such as uninterruptible power supplies

(UPS) do not provide them. Figure 2b adds the service-life dimension: RUL estimation is needed only when the wear-out risk becomes relevant, which may be in the later stage of the designed service life and during a lifetime extension. Monitoring can be scheduled accordingly, which reduces its demands on computation, data storage, and certification for most of the service life.

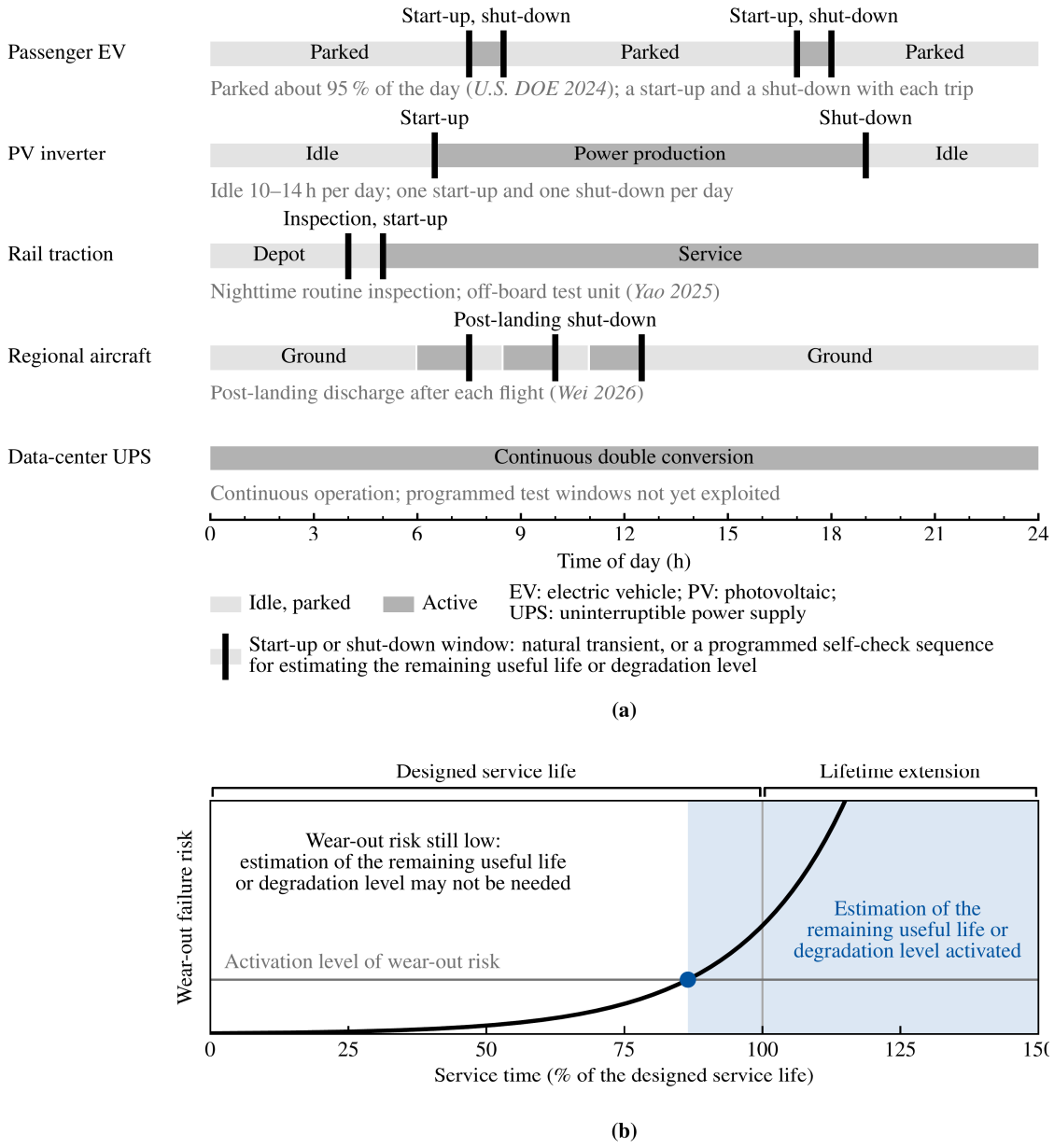


Figure 2. Operation modes and service life. (**a**) Operation modes of five applications on a 24-h axis. Black marks denote start-up and shut-down windows, which are natural transients or can host a programmed self-check. Typical values, not measured duty cycles. (**b**) Estimation of the RUL or degradation level is activated when the wear-out failure risk exceeds an activation level. Studies cited in the figure: refs. [39,43,44].

3.3. Proposed Classification

Figure 3 classifies CM implementations into five hardware categories (rows A–E) and three processing methods (columns 1–3) and lists representative studies [36,42,43,46,48,49,51–76]. In rows A and B, the power stage is not in operation, so monitoring does not affect the operation of the product. Row A would perform a programmed self-check with an auxiliary supply and the existing signal-level circuits. Functional self-tests of this kind exist. Automotive gate drivers include built-in self-tests of their protection comparators and gate-path integrity checks against latent faults [77]. A patented test sequence charges a capacitor, disconnects the gate driver from its supply, drives the gate of the device from the stored charge, and measures the gate charge [78]. None of the studies reviewed for this paper, however, uses such in-system resources to quantify degradation against an EOL margin, and this is the gap that row A denotes. The closest published works add test circuits. These are supplied from

the auxiliary battery and designed to be embedded in the gate drive of an EV inverter [53], or dedicated to a pre-operational switch diagnosis [52]. They belong to row B, together with external injection units [43,51] and a current injection at idle time by circuitry embedded in the gate drive [49]. The boundary of row A is the energized power stage: diagnostic routines that switch the power stage, for example to apply test vectors or to pre-charge the DC link during start-up [46,47], do not qualify and belong to row C. A conceptual row A method could use the isolated supply of an existing gate driver while the DC link remains de-energized. It could measure the gate leakage current of the devices, which together with the threshold voltage indicates gate-oxide degradation [31], or check the integrity of the temperature sensors. Row C changes nothing in the product hardware and uses existing sensors in normal or special operation modes. It is the most scalable route, but it is fully exposed to the cross-sensitivities discussed in Section 5. Row D upgrades existing circuits within the same layout, for example their sensing accuracy or sampling rate, and row E adds dedicated sensing or injection circuits.

	Hardware implementation	Product operation impact	Processing of health indicators (representative literature, non-exhaustive) 1. Model-based	2. Data-driven	3. Hybrid
Offline	**A Offline in-system without additional hardware** Power and auxiliary stages off; self-check with existing circuits	□□□ None	A1–A3 Research gap: no study in the reviewed literature quantifies degradation with in-system resources only; functional self-tests exist in patents and gate-driver ICs. Concept: a programmed self-check before the power stage is energized, using an auxiliary supply and the existing signal-level circuits.		
Offline	**B Offline in-system with additional hardware** Power stage off; external or embedded test circuit	□□□ None	B1 Pre-operational switch diagnostics (*Wu 2026*) Test circuits in the gate drive (*Ji 2015*)	B2 Look-up tables from historical data, with a current injected at idle (*Ji 2013*)	B3 Digital twin solved by the bat algorithm, with signal injection (*Yao 2025*) LC model fitted by the bat algorithm (*Yao 2024*)
Online	**C Online without hardware change** Existing sensors and controller; normal or special modes	■□□ Low	C1 Capacitance from the discharge or start-up profile (*Wei 2024; Wang 2020; Baumann 2024*) Discharge time as a converter-level indicator (*Wei 2026*)	C2 Gaussian-process regression for DC-link capacitors (*Örüklü 2026*) ML-based DC-link capacitor monitoring (*Örüklü 2025*) LSTM-based T_j and damage estimation (*Du 2026a*) Self-commissioning edge anomaly detection (*Gómez 2024*)	C3 ML-aided digital twin (*Wan 2026*) Simulation-to-hardware alignment on shutdown data (*Fassi 2026*) Controller-embeddable probabilistic digital twin (*Milton 2020*)
Online	**D Online with hardware upgrade (same layout)** Upgraded sensing accuracy or sampling rate	■■□ Moderate	D1 Gate-driver-level gate-oxide monitoring (*Naghibi 2025*)	D2 Bond-wire state classification at 10 kHz sampling (*Shen 2025*) Neural network on thermal phase response (*Van Der Broeck 2024*)	D3 PIML parameter estimation (*Zhao 2022*) and digital twin with PSO (*Peng 2021a*), both sampled at twice the switching frequency Embedded digital twin with hybrid RLS (*Wang 2026*)
Online	**E Online with additional hardware** Dedicated sensing or injection circuits	■■■ High	E1 Converter-level and WBG V_{on} circuits (*Peng 2021b; Gill 2025*), also for short-circuit protection (*Liu 2026b*) TSEP decoupling of T_j and bond-wire aging (*Zheng 2026*) Variable electrical network during discharge (*Wu 2019*)	E2 Autoencoder on V_{on} for switch health (*Liu 2026a*) CNN on turn-off voltage for T_j (*Wang 2023*) Time–frequency EMI analysis with ML (*McGrew 2022*)	E3 Physics-guided deep learning on acoustic emission (*Du 2026b*) Digital twin of a DC bank with a Rogowski coil (*Zhu 2023*)

Figure 3. Classification of condition-monitoring methods by hardware implementation (rows A–E) and processing of health indicators (columns 1–3), with cell identifiers such as C2. Row C (blue) requires no hardware change and

is the most scalable route. For row A, no study in the reviewed literature quantifies degradation with in-system resources only. Notation: CNN—convolutional neural network, DC—direct current, EMI—electromagnetic interference, LC—inductor–capacitor, LSTM—long short-term memory, ML—machine learning, PIML—physics-informed machine learning, PSO—particle swarm optimization, RLS—recursive least squares, TSEP—temperature-sensitive electrical parameter, WBG—wide bandgap, T_j—junction temperature, V_{on}—on-state voltage. Studies cited in the figure: refs. [36,42,43,46,48,49,51–76].

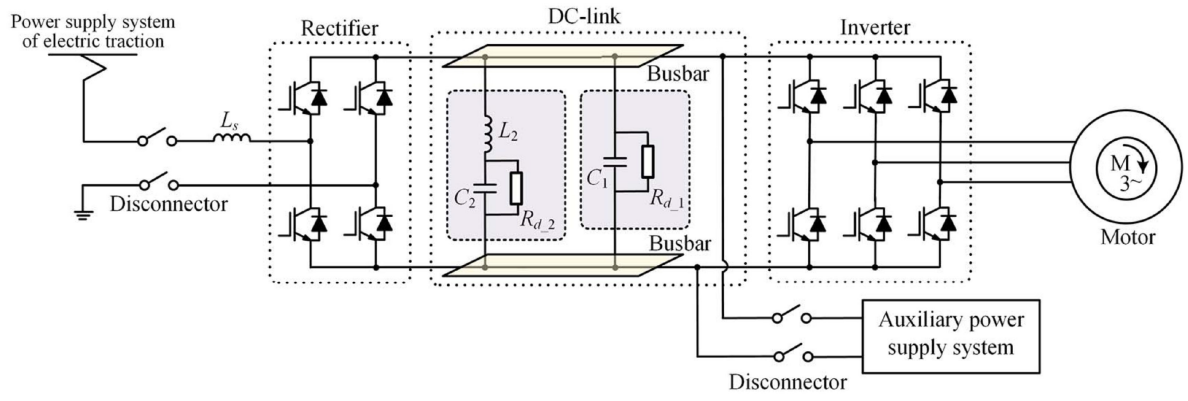
In the reviewed literature, capacitor monitoring is mostly found in row C, because capacitance and equivalent series resistance (ESR) are observable in signals that the converter already measures. Semiconductor monitoring is mostly found in rows D and E, because millivolt changes of the on-state voltage are not. Data-driven and hybrid methods appear in all online rows, including row E [73,75], which indicates that hardware implementation and processing are largely independent attributes. The reliability implication grows from row C to row E, since each added circuit adds a failure path. Neither a parts-count reliability prediction of a CM circuit nor an ISO 26262 diagnostic-coverage analysis of a CM function in a traction inverter [79] is found in the reviewed literature. A pragmatic design principle follows. Methods without hardware modification are preferred as long as the warning window permits. Hardware is added only where it serves a second function, such as protection [70]. Row A deserves investigation, because many converters already provide an auxiliary supply and gate drivers.

3.4. Examples from the Author's Previous Research

Four examples from the author's previous research illustrate representative implementations in rows B to E. Details are given in the cited papers.

3.4.1. Example 1: Injection in the Power-Off State

Traction, wind, and PV converters have power-off windows in which a test signal can be injected without affecting the operation [51]. In railway traction converters, the DC link contains an inductor–capacitor (LC) resonant circuit in parallel with the DC-link capacitor (Figure 4a). A battery-powered hand-held unit is connected during the nighttime inspection (Figure 4b). It superimposes an AC signal on a DC offset, at two excitation frequencies selected from the impedance characteristic of the DC link (Figure 4c). A digital twin solved by the bat algorithm then estimates the DC-link and resonant capacitances concurrently. On a full-scale traction inverter test platform, the average error is below 0.7 % and the maximum error is 1.5 % [43]. A related method estimates the parameters of second- to fourth-order LC networks from the response to a DC step, with errors below 1.6 %, 2.5 %, and 3 %, respectively [51]. Because the converter is de-energized, row B avoids the cross-sensitivity to operating conditions. The price is a maintenance visit and a test unit, but the method can serve as a reference for benchmarking online methods.



(a)

Figure 4. *Cont.*

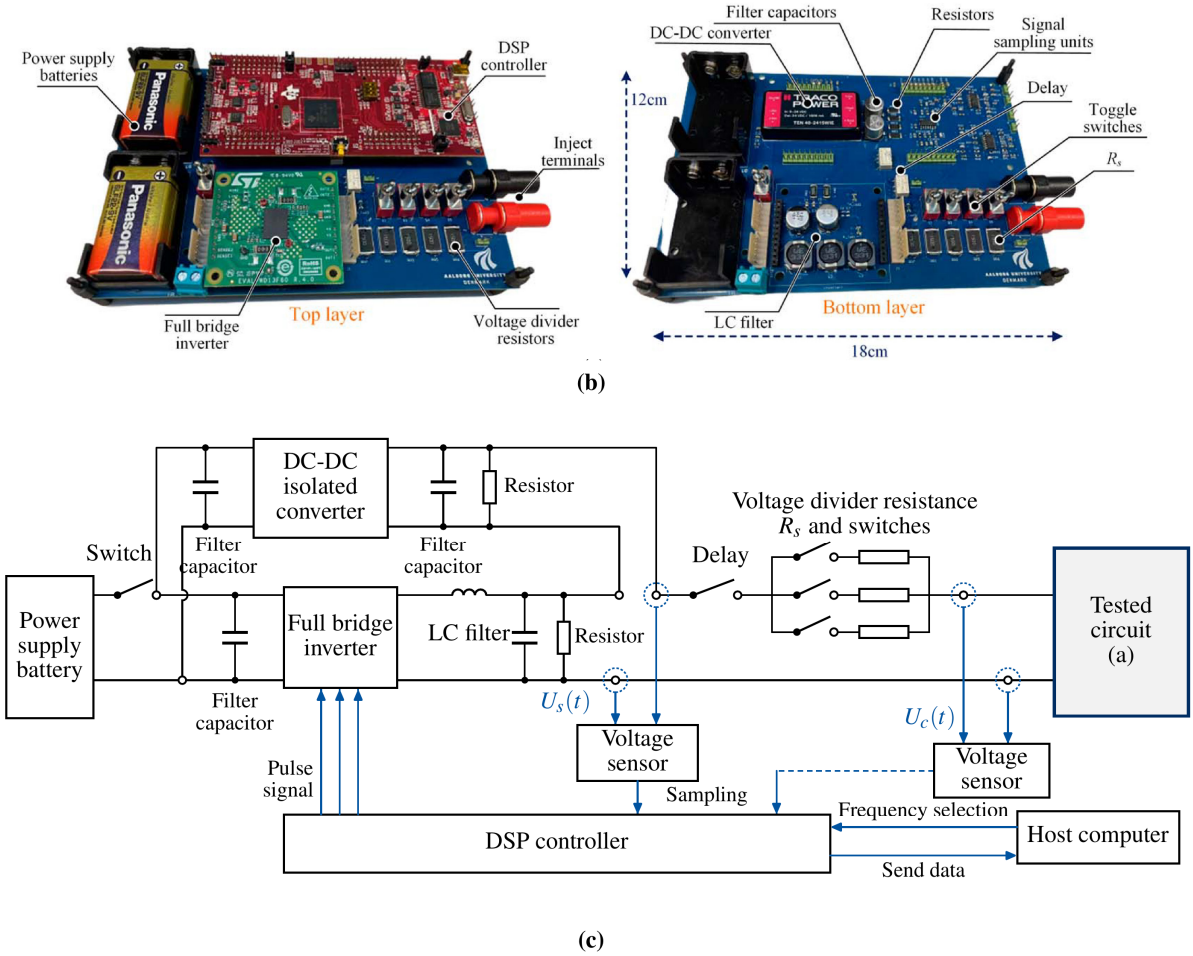
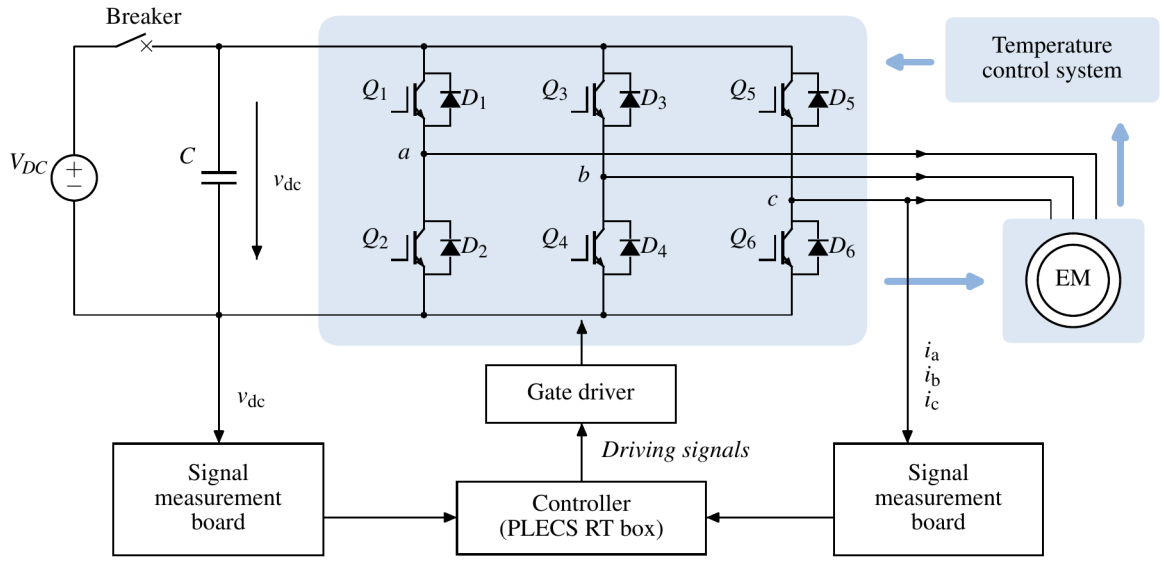


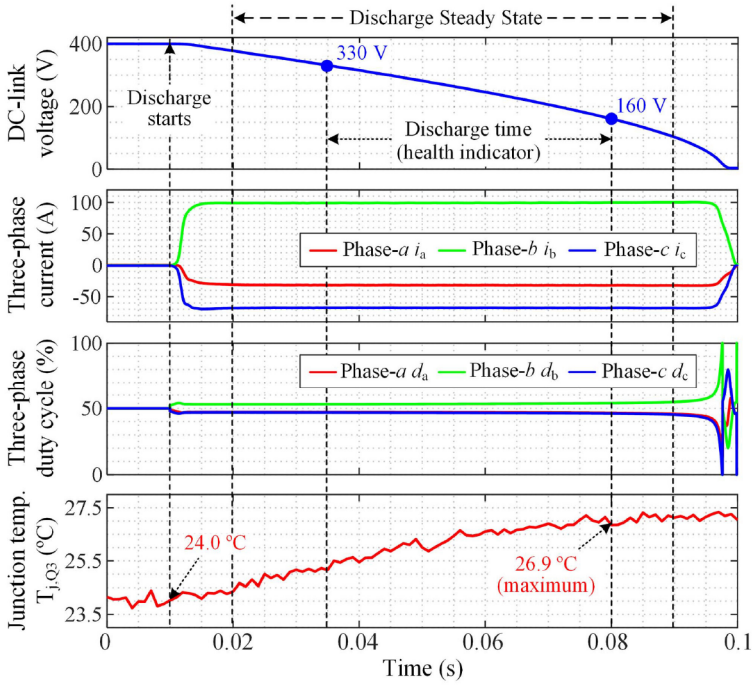
Figure 4. Example 1: condition monitoring of the DC-link capacitors of a railway traction converter in the power-off state [43]. (**a**) Traction converter: DC link with the DC-link capacitor C_1 and the LC resonant circuit (L_2, C_2) between the busbars, the line inductance L_s, and the discharge resistors R_{d1} and R_{d2} [43]. (**b**) Hand-held test unit, top and bottom layers. (**c**) Schematic of the test unit. The output of an isolated DC–DC converter (DC component) in series with the filtered output of a full-bridge inverter (AC component) is injected through a delay switch and the switchable divider resistors R_s. $U_s(t)$ and $U_c(t)$ are the measured injection and tested-circuit voltages, and DSP denotes the digital signal processor. (**a**,**b**) Reprinted with permission from ref. [43]. Copyright 2025, IEEE; (**c**) adapted with permission from ref. [43]. Copyright 2025, IEEE.

3.4.2. Example 2: Discharge Time as a Converter-Level Indicator

In EVs, the inverter or its power stage is usually the smallest replaceable unit, so the primary operational concern is whether the inverter or its power stage needs replacement [42]. The discharge time, measured between two DC-link voltage levels during the mandated discharge after shutdown, answers this question with signals that the inverter already measures (Figure 5). In the current-regulated discharge operation mode, a lower capacitance stores less energy, and a higher on-state resistance dissipates it faster. The degradation of either component therefore shortens the discharge time. In a purely resistive discharge path, a higher resistance would lengthen it instead. The raw discharge times scatter with the rotor angle and the coolant temperature. The method groups the data on a map of these two conditions and normalizes the median of each period to that of the healthy first year of operation. The decision is to be based on the rate of change [42]. The same time window has been used for DC-link capacitance estimation [36,44], power module on-state voltage measurement [50], and a junction-temperature calibration [80]. The limitation is that a converter-level indicator cannot locate the degraded component. It suits cases in which the converter is the smallest replaceable unit.



(a)



(b)

Figure 5. Example 2: discharge time of an EV traction inverter as a converter-level health indicator [42]. (**a**) Test setup with DC source V_{DC}, DC-link capacitor C, inverter switches Q_1–Q_6 with antiparallel diodes D_1–D_6, electric machine (EM), temperature control system, gate driver, controller (PLECS RT Box), and signal measurement boards for the DC-link voltage v_{dc} and the phase currents i_a, i_b, i_c. Adapted with permission from ref. [42]. Copyright 2026, IEEE. (**b**) Experimental discharge waveform after shutdown (d-axis current reference $i_{d,ref}$ = 100 A, initial DC-link voltage 400 V, rotor electrical angle $3\pi/5$, coolant temperature 24 °C): DC-link voltage with the discharge time between 330 and 160 V, phase currents, duty cycles d_a, d_b, d_c, and junction temperature $T_{j,Q3}$ of Q_3. Reprinted with permission from ref. [42]. Copyright 2026, IEEE.

3.4.3. Example 3: Physics-Informed Machine Learning for Circuit Parameter Estimation

Physics-informed machine learning (PIML) estimates the inductance, the capacitance, and the parasitic resistances of a buck converter by coupling a neural network with the dynamic model of the converter (Figure 6) [57]. Intermediate latent states between the observable samples are constrained by the forward and backward equations of the converter model, so that only a small training data set is required, taken from the feedback signals available for control [57]. The processing method is hybrid. Like the digital-twin method of [65], the method requires sampling

the voltage and the current at no less than twice the switching frequency. Depending on whether the existing sensors and signal-conditioning circuits support this sampling rate, the method falls into row C or row D of Figure 3.

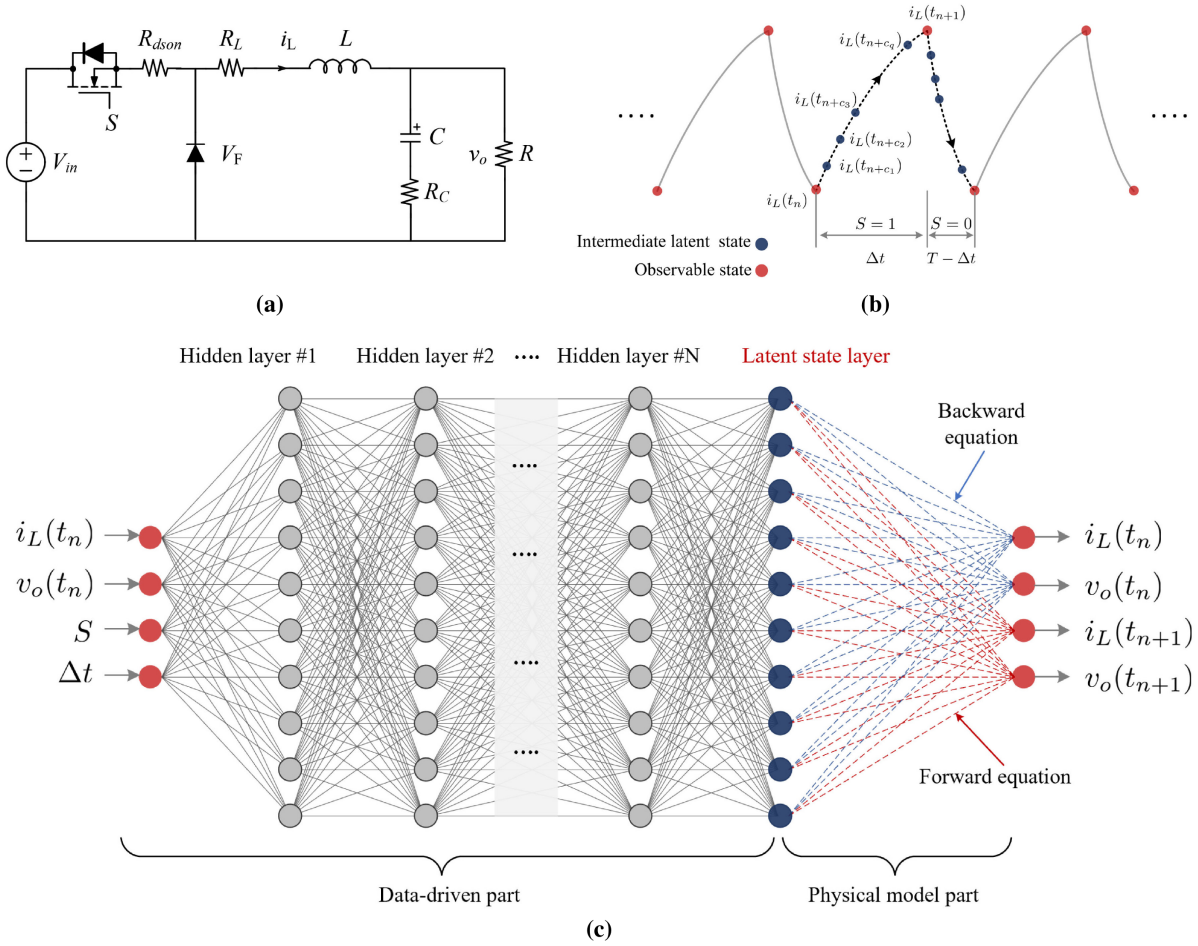


Figure 6. Example 3: parameter estimation of a buck converter with physics-informed machine learning. Reprinted from ref. [57] (open access). (**a**) Buck converter with input voltage V_{in}, switch S with on-state resistance R_{dson}, diode forward voltage V_F, inductor L with resistance R_L and current i_L, capacitor C with ESR R_C, load R, and output voltage v_o. (**b**) Observable states at the sampling instants t_n and intermediate latent states within the switching period T, with the on-time Δt ($S = 1$). (**c**) Network with a data-driven part (hidden layers #1 to #N and a latent state layer) and a physical-model part (forward and backward equations of the converter).

3.4.4. Example 4: Converter-Level On-State Voltage Measurement

The on-state voltage is one of the most widely used health indicators of power semiconductors, but its degradation-related changes amount to tens of millivolts and have to be extracted from a switching voltage of hundreds of volts. One measurement unit connected to the phase-leg midpoints can measure the on-state voltages of all devices of an inverter, as first demonstrated for a single-phase inverter [81]. A self-power scheme removed the external supply [82]. Zener-clamped depletion MOSFETs then reduced the component count and the number of input–output terminals (Figure 7). The demonstrated error is below 0.08 % of full scale, i.e., at most 4 mV, over a ±5 V input range [68]. Added hardware can thus be kept small at the converter level and can serve a second purpose, such as short-circuit protection [70]. The measured on-state voltage still depends on the heat-sink temperature [68], which has to be separated from the degradation. For example, a 5 % increase as the threshold at an on-state voltage of 2 V corresponds to 100 mV. The temperature coefficient of the on-state voltage depends strongly on the load current and changes sign between low and high currents [13]. With a temperature coefficient of about 2.5 mV/K, derived from an increase of about 50 mV for a 20 K rise of the heat-sink temperature [82], a junction-temperature uncertainty of 5 K contributes about 12 mV. Even a fluctuation of the peak current by about ±1 % changes the extracted value by about 10 mV [68]. This cross-sensitivity, not the circuit error, limits the detection.

The four examples cover the right-hand part of Figure 3. Example 1 (row B) uses an external unit in the power-off state and a digital twin fitted by the bat algorithm, i.e., hybrid processing (cell B3). Example 2 (row C) uses existing sensors in a special operation mode and a model-based converter-level indicator (cell C1). Example

3 uses hybrid processing and requires sampling at no less than twice the switching frequency, which places it in cell D3, or in cell C3 if the existing sampling circuit already supports this sampling rate. Example 4 (row E) adds a measurement unit for a model-based indicator (cell E1). From Example 1 to Example 4, the hardware effort and the exposure to the operating conditions increase, while the warning window remains the long-horizon band of Figure 1 in all four cases.

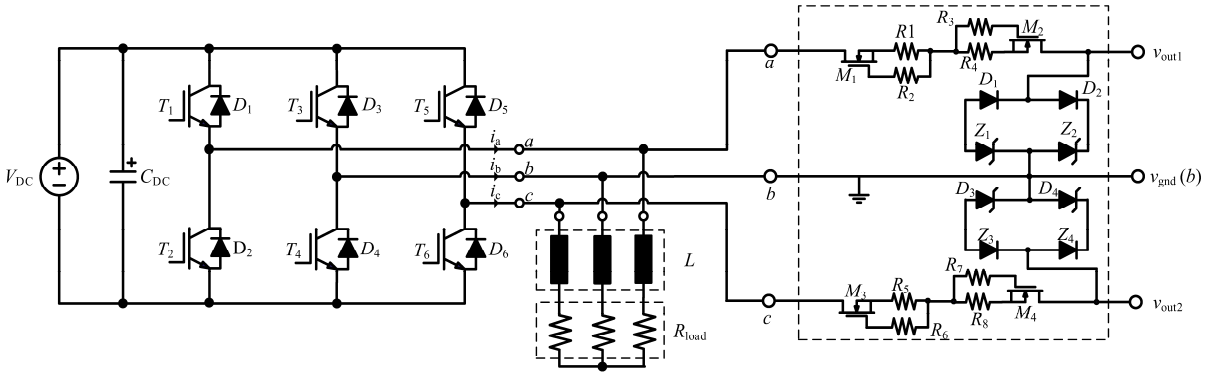


Figure 7. Example 4: converter-level on-state voltage measurement for a three-phase inverter [68]. Inverter with DC voltage V_{DC}, DC-link capacitor C_{DC}, IGBTs T_1–T_6, diodes D_1–D_6, and inductive–resistive load (L, R_{load}). The measurement unit, connected to the phase-leg midpoints a, b, c, contains depletion MOSFETs M_1–M_4, resistors R_1–R_8, and two bridges of diodes (D_1–D_4 of the measurement unit) and Zener diodes (Z_1–Z_4). Crossing wires without a dot are not connected. The outputs v_{out1} and v_{out2}, referred to v_{gnd} at phase b, contain the on-state voltages of all devices, and the DC-link voltage is clamped at the Zener level. Adapted with permission from ref. [68]. Copyright 2021, IEEE.

4. End-of-Life Criteria

EOL determines when a monitoring result should trigger an action, yet it is rarely defined explicitly. This section proposes three EOL criteria on the normalized change of a health indicator and states how the RUL should be reported with its confidence.

Because RUL is the time from the present to the EOL, its value depends on how the EOL is defined. Most CM studies adopt a fixed drift threshold without justifying it, and few state the uncertainty of their prediction. Figure 8 proposes a definition based on the normalized change of a health indicator y,

$$\delta = \left|\frac{\Delta y}{y_0}\right| = \frac{|y - y_0|}{|y_0|}. \tag{1}$$

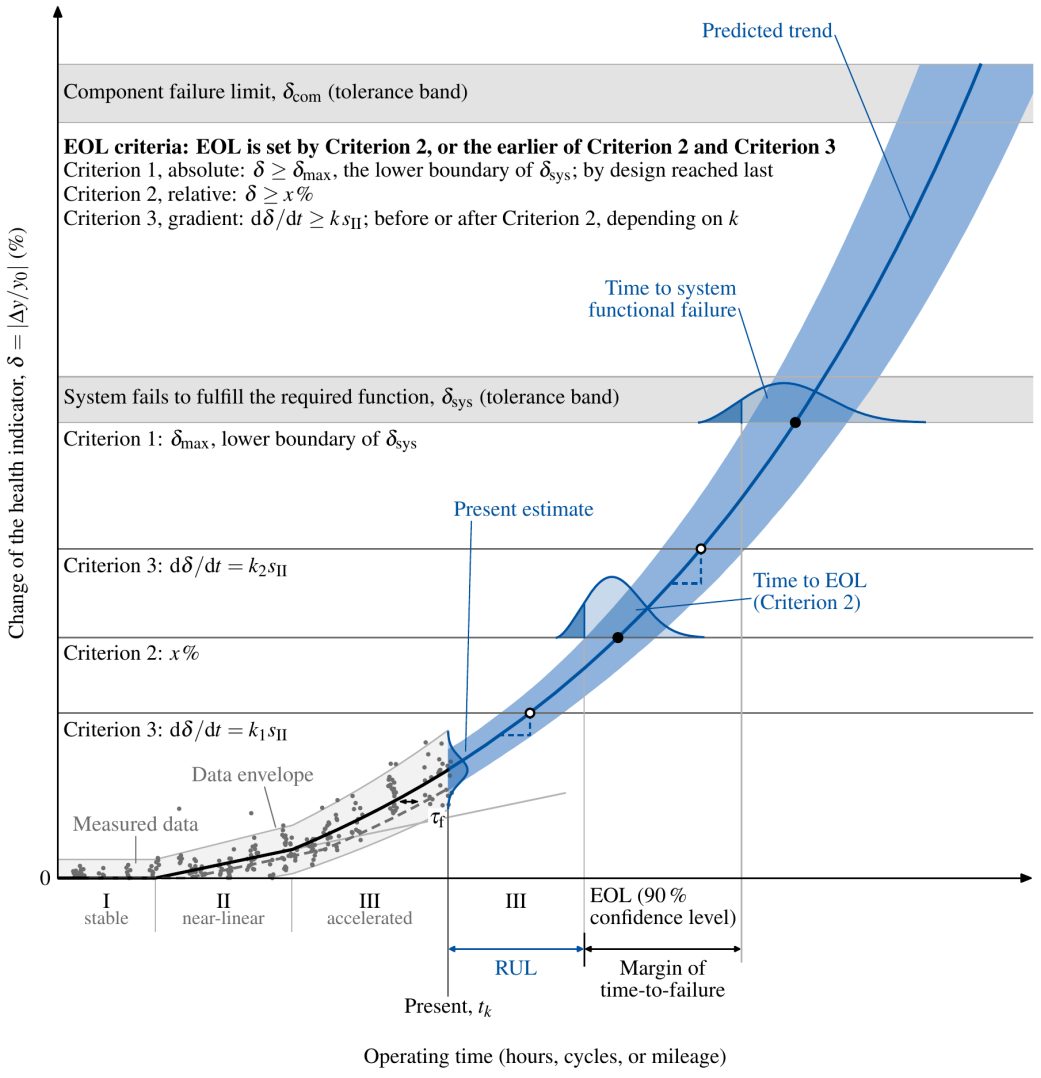
where y_0 is the initial value of the unit. The definition applies to indicators that increase with aging, such as the on-state voltage or the ESR, and to indicators that decrease, such as the capacitance. All criteria are applied to the trend of δ estimated from the scattered measurements. The absolute value is used because each indicator degrades in a known direction. A change against that direction, such as a temporary ESR decrease, is treated as an anomaly rather than as progress toward EOL.

Criterion 1 (absolute) is met when $\delta \geq \delta_{max}$, where δ_{max} is the lower boundary of the tolerance band of δ_{sys}, the change at which the system can no longer fulfill its required function. The system limit follows from the application, for example from the ripple voltage that a reduced DC-link capacitance still allows. It forms a band because it varies across a production population, and its lower boundary is taken at a stated confidence level. The component failure limit δ_{com}, at which the component itself fails, lies above the system limit. A system should be designed so that δ_{max} exceeds the relative threshold of Criterion 2. For a monotonic $\delta(t)$, Criteria 2 and 3 then trigger before Criterion 1.

Criterion 2 (relative) is met when $\delta \geq x\%$. Typical thresholds are a 20 % decrease of the capacitance or a doubling of the ESR for electrolytic capacitors [9] and a 5 % decrease of the capacitance for film capacitors in traction DC links [43]. For power modules in power cycling, the threshold is a 5 % increase of the on-state voltage or a 20 % increase of the thermal resistance [83]. A relative threshold is insensitive to the unit-to-unit variation of y_0, which is why methods intended for field use normalize each unit to its own healthy baseline [42,44]. The value of x has to leave a margin of time-to-failure before Criterion 1 is reached.

Criterion 3 (gradient) is met when $\mathrm{d}\delta/\mathrm{d}t \geq k\, s_{II}$, where s_{II} is the slope of δ in stage II and $k > 1$ is a multiplication factor [84]. Trend-based alarms are established in machinery condition monitoring [19]. The gradient criterion adds the normalization by s_{II} and the deduction of the filter delay (τ_f in Figure 8). The criterion detects the onset

of the accelerated stage independently of the absolute sensitivity of the indicator, which matters for converter-level indicators that respond differently to different components. It is introduced with a case study on IGBT modules in power cycling tests [84]. The discharge-time method of Section 3.4 proposes it for a converter-level indicator, with k as a multiple of the stage-II rate of change. Depending on k, Criterion 3 is reached before or after Criterion 2 (k_1 and k_2 in Figure 8), so the EOL is set by whichever of Criteria 2 and 3 is reached first. Because differentiation amplifies noise, Criterion 3 must be evaluated on a filtered trend, for example on medians of successive periods [42], on a moving-horizon average, or with a Kalman filter that carries the degradation rate as a state. Different values of k imply different margins of time-to-failure. Based on the case study in [84], a value between 3 and 6 is recommended. The gradient-based criterion reduced the inconsistency of the cycle-to-failure among samples from up to 30 % under the 5 % on-state voltage criterion to within 4 %.



Notation

Dots and light-gray band: measured data and their envelope
Black: data trend; dashed: filtered trend, delay τ_f
Gray bands: 90 % tolerance bands of δ_{sys} and δ_{com}
y: health indicator; y_0: its initial value; $\delta = |y - y_0|/|y_0|$
I, II, III: stable, near-linear, and accelerated degradation
s_{II}: slope of stage-II trend (thin gray); $k_1 < k_2$: Criterion 3
t_k: present time; all criteria are applied to the trend of δ
Circles: median trend meets Criteria 1, 2 (filled) and 3 (open)
Blue: present estimate, predicted trend, and its 90 % band
Dashed blue triangle: gradient $k\,s_{II}$ at Criterion 3
EOL: end of life, as set by the EOL criteria
EOL (90 % confidence level): 10 % quantile, dark tail
RUL: remaining useful life, from t_k to this EOL
δ_{max}: lower boundary of δ_{sys}; $x\,\%$: relative threshold
Margin of time-to-failure: EOL to system functional failure
Thin vertical lines: t_k and the 90 % confidence points

Figure 8. EOL criteria and RUL estimation (illustrative). Measured health-indicator data scatter within an envelope. The degradation proceeds through a stable (I), a near-linear (II), and an accelerated stage (III). From the present estimate at t_k, the predicted trend and its 90 % band give the distributions of the time to EOL and to system functional failure, both evaluated at a 90 % confidence level. The tolerance bands of the system limit δ_{sys} and of the component failure limit δ_{com} represent unit-to-unit variation. The time distributions are drawn as right-skewed Weibull densities, as is typical of first-passage times of uncertain trajectories. The horizontal lines of Criterion 3

mark the level of δ at which the slope of the median trend reaches $k_1 s_{II}$ or $k_2 s_{II}$. The criterion itself is evaluated on the gradient.

The predicted trend is uncertain from the present time t_k onward, because the present state is itself an estimate. The time to EOL is therefore a distribution. Stating the EOL at a 90 % confidence level, i.e., at the 10 % quantile of the predictive distribution of the time to EOL (denoted RUL_{10}), gives the RUL a defined meaning. The margin of time-to-failure then extends from this EOL to Criterion 1 at the same confidence level. Prognostic metrics evaluate how early a predicted RUL distribution comes within an allowable error of the true EOL and whether it stays within a narrowing error bound as the EOL approaches [85]. Few CM studies report them. Exceptions give the uncertainty of each prediction [54] or update a lifetime model with in-situ data [86].

5. Limitations in Existing Performance Verifications

A monitoring method can be trusted only as far as its performance has been verified. This section formulates the relation between health indicators and degradation, shows why the prevailing verifications establish sensitivity but not the inverse relation that monitoring requires, and states what a sufficient verification would contain.

5.1. Forward and Inverse Relations

A health indicator depends on the operating conditions and on the state of other components as well as on the degradation of interest. The i-th of m measured health indicators can be written as

$$y_i = f_1\left(\underbrace{x_1, x_2, \ldots, x_p}_{\substack{\text{operating and}\\ \text{environmental conditions}}} , \underbrace{h_1, h_2, \ldots, h_q}_{\substack{\text{health states of other components}\\ \text{(including sensors) or other}\\ \text{degradation mechanisms}}} , \underbrace{\mathrm{Deg}_1, \mathrm{Deg}_2, \ldots, \mathrm{Deg}_n}_{\substack{\text{degradation states}\\ \text{of interest}}} \right), \quad i = 1,2,\ldots,m \tag{2}$$

where f_1 is the physical mapping from the conditions and states to the i-th health indicator, $\mathbf{x} = (x_1, \ldots, x_p) \in \mathcal{X}$ collects the operating and environmental conditions over the field operating domain $\mathcal{X}$, such as the load current, the DC-link voltage, and the ambient and coolant temperatures. The vector $\mathbf{h} = (h_1, \ldots, h_q) \in \mathcal{H}$, where $\mathcal{H}$ is the set of possible health states, collects the health states of the other components, including the sensors, and of other degradation mechanisms, and $\mathbf{h}_0$ denotes that all of them are healthy. The quantities $\mathrm{Deg}_1, \ldots, \mathrm{Deg}_n$ are the n degradation states of interest. A sensor drift thus enters (2) through $\mathbf{h}$ and can mimic degradation. The two vectors are also coupled. A degraded thermal interface or heat sink belongs to $\mathbf{h}$, but it raises the junction temperature, which most methods treat as an operating condition in $\mathbf{x}$. A drifting current sensor likewise changes the estimated load. Compensating $\mathbf{x}$ with measured temperatures or currents can thus absorb part of a degradation that should have been detected. Condition monitoring requires the inverse relation

$$\widehat{\mathrm{Deg}}_i = f_2\left(\underbrace{x_1, x_2, \ldots, x_p}_{\substack{\text{measured, estimated, or}\\ \text{unknown, to be decoupled}}} , \underbrace{h_1, h_2, \ldots, h_q}_{\substack{\text{usually unknown, to be}\\ \text{decoupled if necessary}}} , \underbrace{y_1, y_2, \ldots, y_m}_{\substack{\text{measured or estimated}\\ \text{health indicators}}} \right), \quad i = 1,2,\ldots,n \tag{3}$$

where f_2 is the model-based, data-driven, or hybrid estimator that infers the degradation states from the health indicators, and the hat denotes an estimate of the true state Deg_i. Whether $\mathbf{h}$ has to be decoupled depends on the objective of the monitoring. Decoupling is required when the objective is to separate degradation mechanisms or to locate the degraded component. A converter-level objective may not require it.

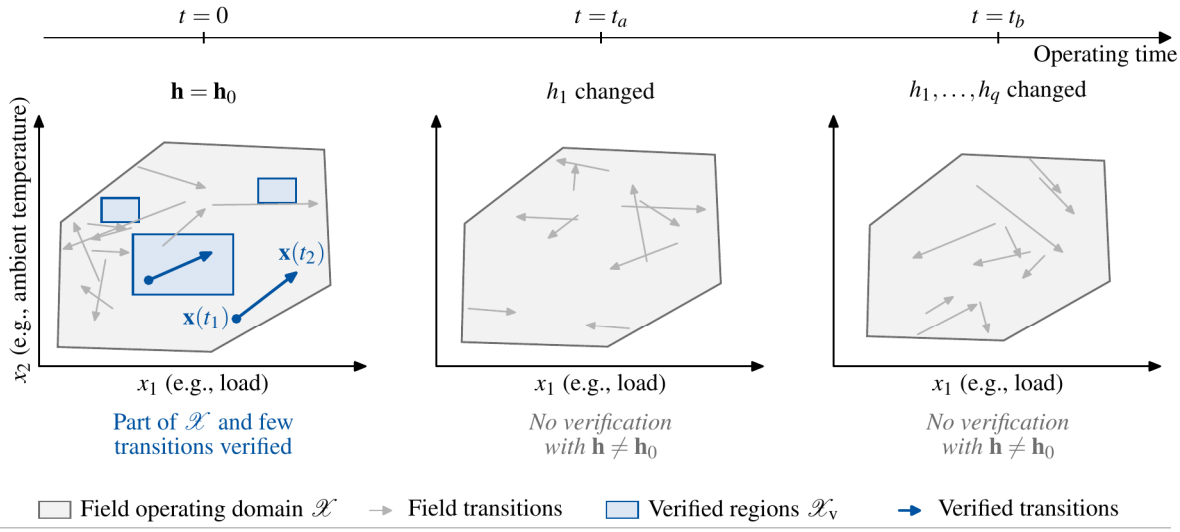
5.2. Sensitivity Is Necessary but Not Sufficient

Most verifications demonstrate that a health indicator changes with degradation. This establishes only the sensitivity of (2). Sensitivity is necessary, but it is not sufficient for the inverse relation (3). To first order, the change caused by the degradation during the monitoring interval must exceed the combined change caused by $\mathbf{x}$, $\mathbf{h}$, and the other degradation states, unless these are measured and compensated. The examples of Section 3.4 illustrate each case. Two capacitances are separated by injecting at two frequencies at which the impedance of the DC link responds differently to them [43]. The discharge time depends on two degradation states and on the rotor angle and the coolant temperature [42]. In Example 3, the component parameters are estimated jointly as unknowns of the converter model [57]. The on-state voltage depends on the temperature and the load current as well as on the

degradation [68]. In each case, the decoupling is part of the method, so a verification has to vary the quantities to be decoupled.

5.3. Narrow Verification

Existing studies usually verify (3) on a small subset $\mathcal{X}_v \subset \mathcal{X}$, typically a few load points at one or a few temperatures. They include few dynamic transitions, such as load steps or thermal transients, and almost always assume $\mathbf{h} = \mathbf{h}_0$ (Figure 9). The performance outside $\mathcal{X}_v \times \mathbf{h}_0$ remains unknown. The few studies with field data show why this matters. A discharge-based capacitor method is evaluated with data from 153 power converters at the European Organization for Nuclear Research (CERN) [48]. A post-fault analysis of a medium-voltage converter found a relevant parameter shift in IGBTs that had apparently survived the fault, which basic tests may not reveal [5]. The static and dynamic characteristics of IGBT modules aged in locomotive service did not reveal their health state, which only power cycling tests separated [6]. Laboratory power cycling tests under non-constant stress, which is common in practical applications, show that degradation can proceed in jumps rather than smoothly [87]. Field data from wind turbines further show that humidity and contamination, design and quality issues, and human errors play an important part in converter failure. Thermal-cycling fatigue of bond contacts and die-attach solder is found not to be a relevant contributor in that application [3].



Notation: x_1, x_2 – operating and environmental conditions, e.g., load and ambient temperature; $\mathbf{x}(t_1), \mathbf{x}(t_2)$ – operating conditions at the start and end of a transition; $\mathcal{X}$ – field operating domain; $\mathcal{X}_v$ – verified regions; $\mathbf{h} = (h_1, \ldots, h_q)$ – health states of other components (including sensors) or other degradation mechanisms; $\mathbf{h}_0$ – all of them healthy; t_a, t_b – later operating times.

Figure 9. Limitations of existing verifications along the operating time (illustrative). At $t = 0$, with $\mathbf{h} = \mathbf{h}_0$, verification typically covers only part of the field operating domain $\mathcal{X}$, spanned here by two example conditions, and a few dynamic transitions. Later, the health states of other components and degradation mechanisms change, and the domain narrows with aging and derating. Verification with $\mathbf{h} \neq \mathbf{h}_0$ is rarely reported.

For data-driven and hybrid methods, the limitation grows with the operating time. A trained f_2 does not wear out, but its accuracy degrades under covariate shift, when $\mathbf{x}$ leaves the training region, and under concept drift, when the underlying physical mapping f_1 shifts continuously as $\mathbf{h}$ evolves. Both call for continuous detection. Two further causes are step changes rather than drifts: a firmware or control update changes f_1 at a known instant and calls for revalidation, and unit-to-unit variation makes f_1 differ across a fleet. Normalizing each unit to its initial value (Section 4) removes only the static part of this variation, not the difference in the degradation trajectory, which requires per-unit calibration or adaptive learning. Uncertainty quantification with the detection of out-of-distribution inputs, periodic recalibration in special operation modes, self-commissioning learning [63], and physics-informed constraints [57] can mitigate this degradation.

5.4. Toward Sufficient Verification

A sufficient verification would state the covered part of $\mathcal{X}$ and the dynamic operations tested. It would vary the health states of the other components and sensors that the method claims to decouple, and it would use more than one unit. It would report the error of $\widehat{\mathrm{Deg}}_i$ with its uncertainty and the false-alarm and missed-detection rates

at the criteria of Section 4. Where possible, it would compare with field data. Decision metrics at a defined EOL criterion are rarely reported. Data-driven studies report classification accuracy, confusion matrices, or the area under the receiver operating characteristic [59,63], but few report false-alarm or missed-detection rates at such a criterion, or detection lead times. One example is a wire-bond pre-warning issued 15 % to 20 % of the lifetime before the EOL criterion without false positives [88]. Special operation modes reduce the verification effort by fixing part of **x** by design, but the remaining conditions still have to be compensated.

6. Operation Optimization: Measures and Limitations

Active thermal control (ATC) [89,90] and its lifetime-oriented variants [91,92] have been reviewed in [93]. The measures of ATC have been mapped onto time scales from the gate driver to the system [94]. Figure 10 extends this map with the side effects of each measure and with non-thermal measures.

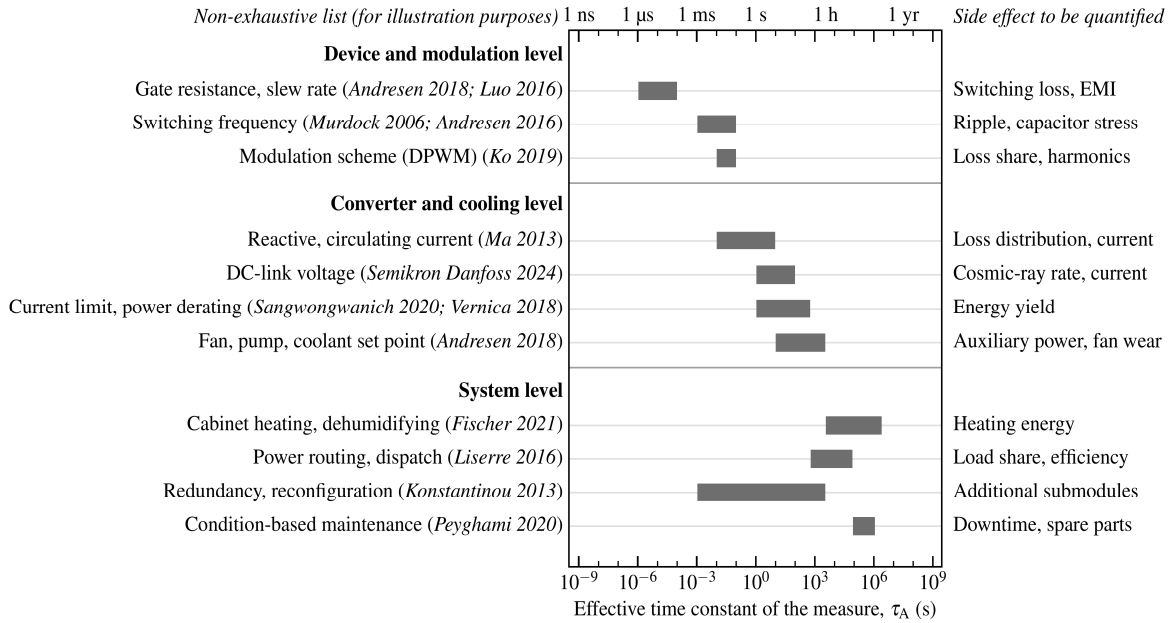


Figure 10. Measures of reliability-oriented operation on the time axis of Figure 1 (non-exhaustive, for illustration). Gray bars show the indicative effective time constant τ_A of each measure, and the right column names the side effect that should be quantified. The layout extends the time-scale map of [94], which assigns time steps of about 1 µs, 100 µs, 1 ms, and 10 ms to the gate driver, the modulator, the converter controller, and the system controller. The time constants are indicative. References give representative studies, e.g., of gate driving [95] and discontinuous pulse-width modulation (DPWM) [96]. Studies cited in the figure: refs. [4,89–92,94–101].

A measure is effective only if its time constant is shorter than the period of the stress it targets (Figure 10) and if the cost of the losses it adds is smaller than the cost of the damage it avoids. The cost–benefit analysis in [94] shows that active thermal control is most cost-effective for large thermal swings in short periods, whereas compensating long-period cycles requires high additional losses. Slow stress therefore calls for slow measures, such as derating, power routing [97], redundancy [98], and maintenance scheduling [99]. The time scale of the degradation in Figure 1 should not be confused with the execution rate of the monitoring algorithm. A slowly evolving health state can be estimated at a high rate and passed to a fast measure, provided that the time constant of the measure matches the period of the stress it targets.

Most measures transfer thermal or electrical stress to other components. Switching-frequency control reduces a temperature swing at the cost of additional losses, a higher current ripple, and a higher stress on the passive components [94]. Reactive-current injection changes the distribution of the losses among the devices and increases the converter current [100]. A lower DC-link voltage reduces the cosmic-ray failure rate, which depends quasi-exponentially on the voltage, but, at the same power, increases the current [101]. Few evaluations report both the benefit and the penalty. In one of them, switching-frequency control reduced the accumulated damage to 72 % of the uncontrolled value at the cost of a 9.7 % increase in energy loss, but the effect on the passive components is not quantified [94]. Return-on-investment indicators have also been used to weigh the lifetime gain against the efficiency or power-quality penalty [93]. Each measure would need to report the side effects listed in the right column of Figure 10.

Operation and monitoring interact. A controller that flattens the temperature swing removes the excitation needed for thermal-impedance-based detection, and a controller that changes the operating point changes **x** in (2). Health indicators should therefore be acquired in windows before an action, such as the special operation modes of Figure 2. Health-aware modulation and power routing, which redistribute the loading of smart-transformer modules, parallel converters, or dual-active-bridge switches according to the estimated degradation, have been demonstrated in simulations and laboratory prototypes [102–104]. They are the most direct link between the classification of Section 3 and operation optimization, because the health indicator of a row C or row D method becomes an input of the modulator. No field validation has been reported in these studies, however, and none of these controllers propagates the uncertainty of the health estimate into the control law.

The measures are not aligned with the dominant field failure causes either. Most measures in Figure 10 target thermal cycling, whereas field data from wind turbines point to humidity as a critical stressor and likely driver of converter failure [3,4]. In that application, measures against humidity and condensation, such as cabinet heating, address the main stressor, although failures at restart occurred even in turbines with converter preheating routines [3]. Falck et al. noted in 2018 that commercial use of ATC had not been reported [1], and evidence on its life-cycle cost remains scarce [93,105].

7. Conclusions and Research Directions

Health indicators and monitoring methods for power electronics are documented extensively, but industrial deployment remains limited. This paper has related the gap to five causes and proposed a perspective for each. The feasible monitoring function is set by the time available to detect and to act. Deployability depends largely on the hardware implementation, which should be assessed separately from the processing method. EOL criteria are rarely justified or stated with a confidence level. Most verifications demonstrate the sensitivity of a health indicator, whereas monitoring requires the inverse relation to hold over the field operating domain. Operation optimization approaches are usually assessed by their benefit for one component, and the stress they shift to others is seldom quantified. The perspectives suggest the following research directions:

(1) Develop CM methods that give pre-warning of short-time-scale failures, from seconds to days, such as an imminent short circuit of an aluminum electrolytic capacitor after overvoltage or ripple overload (Figure 1). Such failures are often unrelated to long-term wear-out, but they have severe consequences if no action is taken before the catastrophic event. The limited time window makes them challenging.

(2) Develop CM methods without hardware change and with online learning. Such methods promise a close-to-zero initial adoption cost, scalability, and continuous monitoring, and they need neither hardware modification nor offline training data. When a new product enters field operation, an algorithm learns the healthy baselines of the components or the converter during the first period of operation. Over the service life, the baselines are kept or updated, and abnormalities or severe degradation are detected from the changes of the health indicators relative to the baselines. As field data accumulate from many converters, offline training becomes feasible and can refine the online models of each converter. This line of methods lowers the barrier to implementation.

(3) Explore application-specific CM methods that use special operation modes and programmed self-checks, with much lower requirements on implementation and on the processing of health indicators.

(4) Propose more comprehensive and relevant EOL criteria. An EOL criterion is more than a fixed percentage change of one health indicator, as widely used in academic publications and industry reports. Figure 8 outlines a broader perspective. In practice, a more elaborate decision procedure may be needed to improve the monitoring accuracy and to reduce false alarms, which remains to be investigated and demonstrated. A framework for refining the EOL criteria and the decision procedure, in laboratory testing and over the service life in the field, is also needed.

(5) Develop better frameworks and procedures to demonstrate and verify the performance of diagnosis and prognosis methods. Both fault diagnosis and CM methods in the literature face the limitations discussed in Section 5. Without sufficient verification, the performance of most, if not all, reported methods remains unconfirmed. Although new health indicators and their measurement or estimation methods keep appearing, this long-standing gap has not been addressed. A better verification framework is essential for fair benchmarking and for industrial deployment.

(6) Explore further opportunities in operation optimization and investigate their system-level (application-level) impact and the competing solutions.

8. Biographies of the Authors



Huai Wang is a Professor at the Department of Energy (AAU Energy), Aalborg University, Denmark, where he has worked since 2012 and has held his current position since 2019. He leads the Reliability of Power Electronic Converters (ReliaPEC) research group and chairs the Mission on Digital Transformation and AI at AAU Energy. His research focuses on efficient, reliable, and cognitive power electronic converters. He has given more than 100 invited talks and collaborates widely with universities and industry across the power electronics value chain. He received his B.E. from Huazhong University of Science and Technology (2007) and his Ph.D. from City University of Hong Kong (CityUHK, 2012), and has held visiting positions at ABB Corporate Research (2009), MIT (2012), and ETH Zurich (2013). He received the IEEE PELS Richard M. Bass Outstanding Young Power Electronics Engineer Award (2016) and was elected a member of the Danish Academy of Technical Sciences (2023).

Funding

This research received no external funding.

Institutional Review Board Statement

Not applicable.

Informed Consent Statement

Not applicable.

Data Availability Statement

No new data were created or analyzed in this study. Data sharing is not applicable to this article.

Conflicts of Interest

The author declares no conflict of interest.

Use of AI and AI-Assisted Technologies

During the preparation of this work, the author used Claude (Anthropic) to assist with language editing. After using this tool, the author reviewed and edited the content as needed and takes full responsibility for the content of the published article.

References

1. Falck, J.; Felgemacher, C.; Rojko, A.; et al. Reliability of Power Electronic Systems: An Industry Perspective. *IEEE Ind. Electron. Mag.* **2018**, *12*, 24–35. https://doi.org/10.1109/mie.2018.2825481.
2. Yang, S.; Bryant, A.; Mawby, P.; et al. An industry-based survey of reliability in power electronic converters. *IEEE Trans. Ind. Appl.* **2011**, *47*, 1441–1451. https://doi.org/10.1109/TIA.2011.2124436.
3. Fischer, K.; Pelka, K.; Puls, S.; et al. Exploring the Causes of Power-Converter Failure in Wind Turbines based on Comprehensive Field-Data and Damage Analysis. *Energies* **2019**, *12*, 593. https://doi.org/10.3390/en12040593.
4. Fischer, K.; Steffes, M.; Pelka, K.; et al. Humidity in Power Converters of Wind Turbines—Field Conditions and Their Relation with Failures. *Energies* **2021**, *14*, 1919. https://doi.org/10.3390/en14071919.
5. Ferreira, G.S.; Lopes, V.H.S.; Rocha, A.V.; et al. Postfault Degradation Analysis of IGBT Power Devices in Medium Voltage Converters. *IEEE Trans. Ind. Appl.* **2025**, *61*, 3597–3607. https://doi.org/10.1109/tia.2025.3531823.
6. Lai, W.; Shangguan, M.; Shi, J.; et al. Research on Remaining Lifetime Evaluation for Traction System IGBT Devices of Electric Locomotives with Different Service Mileage. *IEEE Trans. Power Electron.* **2025**, *40*, 6020–6032. https://doi.org/10.1109/tpel.2024.3518062.
7. Yang, S.; Xiang, D.; Bryant, A.; et al. Condition Monitoring for Device Reliability in Power Electronic Converters: A Review. *IEEE Trans. Power Electron.* **2010**, *25*, 2734–2752. https://doi.org/10.1109/tpel.2010.2049377.
8. Avenas, Y.; Dupont, L.; Baker, N.; et al. Condition Monitoring: A Decade of Proposed Techniques. *IEEE Ind. Electron. Mag.* **2015**, *9*, 22–36. https://doi.org/10.1109/mie.2015.2481564.
9. Wang, H.; Blaabjerg, F. Reliability of Capacitors for DC-Link Applications in Power Electronic Converters—An Overview. *IEEE Trans. Ind. Appl.* **2014**, *50*, 3569–3578. https://doi.org/10.1109/tia.2014.2308357.

10. Soliman, H.; Wang, H.; Blaabjerg, F. A Review of the Condition Monitoring of Capacitors in Power Electronic Converters. *IEEE Trans. Ind. Appl.* **2016**, *52*, 4976–4989. https://doi.org/10.1109/tia.2016.2591906.
11. Zhao, Z.; Davari, P.; Lu, W.; et al. An Overview of Condition Monitoring Techniques for Capacitors in DC-Link Applications. *IEEE Trans. Power Electron.* **2021**, *36*, 3692–3716. https://doi.org/10.1109/tpel.2020.3023469.
12. Oh, H.; Han, B.; McCluskey, P.; et al. Physics-of-Failure, Condition Monitoring, and Prognostics of Insulated Gate Bipolar Transistor Modules: A Review. *IEEE Trans. Power Electron.* **2015**, *30*, 2413–2426. https://doi.org/10.1109/tpel.2014.2346485.
13. Avenas, Y.; Dupont, L.; Khatir, Z. Temperature Measurement of Power Semiconductor Devices by Thermo-Sensitive Electrical Parameters—A Review. *IEEE Trans. Power Electron.* **2012**, *27*, 3081–3092. https://doi.org/10.1109/tpel.2011.2178433.
14. Baker, N.; Liserre, M.; Dupont, L.; et al. Improved Reliability of Power Modules: A Review of Online Junction Temperature Measurement Methods. *IEEE Ind. Electron. Mag.* **2014**, *8*, 17–27. https://doi.org/10.1109/mie.2014.2312427.
15. Zhao, S.; Blaabjerg, F.; Wang, H. An Overview of Artificial Intelligence Applications for Power Electronics. *IEEE Trans. Power Electron.* **2021**, *36*, 4633–4658. https://doi.org/10.1109/tpel.2020.3024914.
16. Van Der Broeck, C.H.; Kalker, S.; De Doncker, R.W. Intelligent Monitoring and Maintenance Technology for Next-Generation Power Electronic Systems. *IEEE J. Emerg. Sel. Top. Power Electron.* **2023**, *11*, 4403–4418. https://doi.org/10.1109/jestpe.2021.3119590.
17. Wang, H.; Blaabjerg, F. Power Electronics Reliability: State of the Art and Outlook. *IEEE J. Emerg. Sel. Top. Power Electron.* **2021**, *9*, 6476–6493. https://doi.org/10.1109/jestpe.2020.3037161.
18. *IEEE Std 1856-2017*; IEEE Standard Framework for Prognostics and Health Management of Electronic Systems. IEEE: New York, NY, USA, 2017. https://doi.org/10.1109/ieeestd.2017.8227036.
19. *ISO 13381-1:2025*; Condition Monitoring and Diagnostics of Machine Systems—Prognostics—Part 1: General Guidelines and Requirements. ISO: Geneva, Switzerland, 2025.
20. Moubray, J. *Reliability-Centred Maintenance*, 2nd ed.; Industrial Press: New York, NY, USA, 1997.
21. Wu, R.; Diaz Reigosa, P.; Iannuzzo, F.; et al. Study on Oscillations During Short Circuit of MW-Scale IGBT Power Modules by Means of a 6-kA/1.1-kV Nondestructive Testing System. *IEEE J. Emerg. Sel. Top. Power Electron.* **2015**, *3*, 756–765. https://doi.org/10.1109/jestpe.2015.2414448.
22. Wang, Z.; Shi, X.; Tolbert, L.M.; et al. Temperature-Dependent Short-Circuit Capability of Silicon Carbide Power MOSFETs. *IEEE Trans. Power Electron.* **2016**, *31*, 1555–1566. https://doi.org/10.1109/tpel.2015.2416358.
23. Landel, M.; Gautier, C.; Labrousse, D.; et al. Experimental study of the short-circuit robustness of 600 V E-mode GaN transistors. *Microelectron. Reliab.* **2016**, *64*, 560–565. https://doi.org/10.1016/j.microrel.2016.07.042.
24. Zeller, H.R. Cosmic ray induced failures in high power semiconductor devices. *Solid-State Electron.* **1995**, *38*, 2041–2046. https://doi.org/10.1016/0038-1101(95)00082-5.
25. Scheuermann, U.; Schilling, U. Cosmic Ray Failures of Power Modules—The Diode Makes the Difference. In Proceedings of the PCIM Europe, Nuremberg, Germany, 19–21 May 2015; pp. 494–501.
26. Lu, B.; Sharma, S.K. A Literature Review of IGBT Fault Diagnostic and Protection Methods for Power Inverters. *IEEE Trans. Ind. Appl.* **2009**, *45*, 1770–1777. https://doi.org/10.1109/tia.2009.2027535.
27. Gmati, B.; Jlassi, I.; Khojet El Khil, S.; et al. Open-switch fault diagnosis in voltage source inverters of PMSM drives using predictive current errors and fuzzy logic approach. *IET Power Electron.* **2021**, *14*, 1059–1072. https://doi.org/10.1049/pel2.12098.
28. Infineon Technologies AG. *Transient Thermal Measurements and Thermal Equivalent Circuit Models*; Application Note AN2015-10; Infineon Technologies AG: Neubiberg, Germany, 2020.
29. Gómez-Aleixandre, C.; Albella, J.M.; Martínez-Duart, J.M. Pressure Build-Up in Aluminium Electrolytic Capacitors under Stressed Voltage Conditions. *J. Appl. Electrochem.* **1986**, *16*, 109–115. https://doi.org/10.1007/bf01015990.
30. TDK Electronics AG. Aluminum Electrolytic Capacitors: General Technical Information. 2026. Available online: https://www.tdk-electronics.tdk.com/download/530704/11a9011cd3cac4ccfbc490fbd4ce88b4/pdf-generaltechnicalinformation.pdf (accessed on 7 October 2026).
31. Wang, J.; Jiang, X. Review and analysis of SiC MOSFETs' ruggedness and reliability. *IET Power Electron.* **2020**, *13*, 445–455. https://doi.org/10.1049/iet-pel.2019.0587.
32. Wang, H.; Nielsen, D.A.; Blaabjerg, F. Degradation testing and failure analysis of DC film capacitors under high humidity conditions. *Microelectron. Reliab.* **2015**, *55*, 2007–2011. https://doi.org/10.1016/j.microrel.2015.06.011.
33. Bayerer, R.; Herrmann, T.; Licht, T.; et al. Model for power cycling lifetime of IGBT modules—Various factors influencing lifetime. In Proceedings of the 5th International Conference on Integrated Power Electronics Systems, Nuremberg, Germany, 11–13 March 2008; pp. 1–6.
34. He, Y.; Wang, F.; Du, G.; et al. Unveiling first self-healing in metallised film capacitor: A macro–micro analysis. *High Volt.* **2025**, *10*, 362–373. https://doi.org/10.1049/hve2.70005.
35. You, H.; Wei, Z.; Hu, B.; et al. Partial Discharge Behaviors in Power Modules Under Square Pulses with Ultrafast *dv*/*dt*. *IEEE Trans. Power Electron.* **2021**, *36*, 2611–2620. https://doi.org/10.1109/tpel.2020.3014043.

36. Wei, X.; Yao, B.; Peng, Y.; et al. An Improved Discharge Profile-Based DC-Link Capacitance Estimation for Traction Inverter in Electric Vehicle Applications. *IEEE Trans. Power Electron.* **2024**, *39*, 8696–8708. https://doi.org/10.1109/tpel.2024.3383153.
37. Wei, X.; Jin, L.; Yao, B.; et al. Application-Driven Data Acquisition for Condition Monitoring of Power Semiconductors in Traction Inverter Applications. *IEEE Trans. Transp. Electrif.* **2024**, *10*, 6812–6824. https://doi.org/10.1109/tte.2023.3339848.
38. Liu, H.; Zhang, H.S.; Tang, Y. An Improved Fusion Framework of Remaining Useful Life Prediction and Predictive Maintenance for High-Power IGBT Modules. *IEEE Trans. Power Electron.* **2026**, *41*, 5831–5851. https://doi.org/10.1109/tpel.2025.3629387.
39. U.S. Department of Energy. FOTW #1356, August 19, 2024: Household Vehicles Were Parked 95% on a Typical Day in 2022. Available online: https://www.energy.gov/cmei/vehicles/articles/fotw-1356-august-19-2024-household-vehicles-were-parked-95-typical-day-2022 (accessed on 7 October 2026).
40. UNECE. *Uniform Provisions Concerning the Approval of Vehicles with Regard to the Protection of the Occupants in the Event of a Frontal Collision*; UN Regulation No. 94, Annex 11; United Nations Economic Commission for Europe (UNECE): Geneva, Switzerland, 2012; p. 77.
41. Electric-Powered Vehicles: Electrolyte Spillage and Electrical Shock Protection. § 571.305 Standard No. 305. 2025. Available online: https://www.ecfr.gov/current/title-49/subtitle-B/chapter-V/part-571/subpart-B/section-571.305 (accessed on 7 October 2026).
42. Wei, X.; Wang, Z.; Yao, B.; et al. A Converter-Level Health Monitoring Method for Traction Inverter Application. *IEEE Trans. Power Electron.* **2026**, *41*, 9513–9527. https://doi.org/10.1109/tpel.2025.3645484.
43. Yao, B.; Wei, X.; Wang, H.; et al. A Condition Monitoring Method for the DC-Link Capacitors in the Traction Converter System with an LC Resonant Circuit. *IEEE Trans. Ind. Electron.* **2025**, *72*, 14797–14807. https://doi.org/10.1109/tie.2025.3577299.
44. Wei, X.; Yao, B.; Wang, Z.; et al. A Robust Health Monitoring Method for DC-Link Capacitor Banks in Aerospace Motor Drives. *IEEE Trans. Power Electron.* **2026**, *41*, 8392–8408. https://doi.org/10.1109/tpel.2025.3642690.
45. Kim, M.; Sul, S.K.; Lee, J. Condition monitoring of DC-link capacitors in drive system for electric vehicles. In Proceedings of the 2012 IEEE Vehicle Power and Propulsion Conference (VPPC), Seoul, Republic of Korea, 9–12 October 2012; pp. 633–637. https://doi.org/10.1109/vppc.2012.6422642.
46. Wang, Z.; Zhang, Y.; Wang, H.; et al. Capacitor Condition Monitoring Based on the DC-Side Start-Up of Modular Multilevel Converters. *IEEE Trans. Power Electron.* **2020**, *35*, 5589–5593. https://doi.org/10.1109/tpel.2019.2956808.
47. Wu, X.; Li, K.; Yu, T.; et al. A Capacitance Estimation Method for DC-Link Capacitors Based on Pre-Charging Model and Noise Evaluation. *IEEE Trans. Ind. Electron.* **2023**, *70*, 8477–8487. https://doi.org/10.1109/tie.2022.3217587.
48. Baumann, T.F.; Murillo-Garcia, R.; Papastergiou, K.; et al. Discharge-Based Condition Monitoring for Electrolytic DC-Link Capacitors. *IEEE Trans. Power Electron.* **2024**, *39*, 16622–16637. https://doi.org/10.1109/tpel.2024.3442077.
49. Ji, B.; Pickert, V.; Cao, W.; et al. *In Situ* Diagnostics and Prognostics of Wire Bonding Faults in IGBT Modules for Electric Vehicle Drives. *IEEE Trans. Power Electron.* **2013**, *28*, 5568–5577. https://doi.org/10.1109/tpel.2013.2251358.
50. Wei, X.; Wang, Z.; Yao, B.; et al. Discharge Profile-Based Converter-Level Health Monitoring for Power Semiconductor Module in Traction Inverter Application. *IEEE Trans. Power Electron.* **2026**, *41*, 16333–16352. https://doi.org/10.1109/tpel.2026.3682643.
51. Yao, B.; Peng, Y.; Zhang, Y.; et al. An Estimation Method of High-Order *LC* Circuits in Power Electronic Converters. *IEEE Trans. Ind. Electron.* **2024**, *71*, 5274–5284. https://doi.org/10.1109/tie.2023.3285917.
52. Wu, C.C.; Chang-Chien, L.R.; Liang, H.; et al. Pre-Op Diagnostics of Power Switch in Three-Phase Full-Bridge Inverters. *IEEE Trans. Ind. Appl.* **2026**. https://doi.org/10.1109/tia.2026.3678571.
53. Ji, B.; Song, X.; Cao, W.; et al. *In Situ* Diagnostics and Prognostics of Solder Fatigue in IGBT Modules for Electric Vehicle Drives. *IEEE Trans. Power Electron.* **2015**, *30*, 1535–1543. https://doi.org/10.1109/tpel.2014.2318991.
54. Örüklü, K.; Yao, B.; Sangwongwanich, A.; et al. Gaussian Process Regression-Based Condition Monitoring of DC-Link Capacitors in Three-Phase AC/DC/AC Converters. *IEEE Trans. Power Electron.* **2026**, *41*, 13474–13484. https://doi.org/10.1109/tpel.2026.3673870.
55. Örüklü, K.; Ağalar, Ş. Machine Learning-Based Condition Monitoring for DC-Link Capacitors in AC/DC/AC Converters. *IEEE Trans. Ind. Electron.* **2025**, *72*, 4227–4237. https://doi.org/10.1109/tie.2024.3454814.
56. Du, B.; Zuo, Y.; Özel, K.E.; et al. LSTM-Based Junction Temperature Monitoring and Thermal Damage Estimation for SiC MOSFETs. *IEEE Trans. Ind. Appl.* **2026**. https://doi.org/10.1109/tia.2026.3724985.
57. Zhao, S.; Peng, Y.; Zhang, Y.; et al. Parameter Estimation of Power Electronic Converters with Physics-Informed Machine Learning. *IEEE Trans. Power Electron.* **2022**, *37*, 11567–11578. https://doi.org/10.1109/tpel.2022.3176468.
58. Wan, Y.; Xu, Q. Machine Learning-Aided Digital Twin Framework with Noninvasive Parameter Estimation for Voltage Source Converters. *IEEE Trans. Ind. Electron.* **2026**, *73*, 10918–10930. https://doi.org/10.1109/tie.2026.3657019.

59. Fassi, Y.; Zhao, S.; Heiries, V.; et al. Physics-Informed Simulation-to-Hardware Alignement for DC-Link Capacitor Condition Monitoring. *IEEE Trans. Power Electron.* **2026**, *41*, 11388–11399. https://doi.org/10.1109/tpel.2026.3663772.
60. Naghibi, J.; Mohsenzade, S.; Mehran, K.; et al. A Gate Driver-Level Isolated Monitoring Technique for Gate Oxide Degradation in Silicon Carbide Power MOSFETs. *IEEE Trans. Power Electron.* **2025**, *40*, 18178–18188. https://doi.org/10.1109/tpel.2024.3488581.
61. Zheng, D.; Fan, T.; Wen, X.; et al. Decoupling Method for Simultaneous Online Tj and Bond-Wire Aging Monitoring of SiC MOSFETs. *IEEE Trans. Power Electron.* **2026**, *41*, 20853–20858. https://doi.org/10.1109/tpel.2026.3700178.
62. Liu, Y.; Wei, X.; Zhao, S.; et al. Application-Oriented Power Semiconductor Switches Condition Monitoring Based on Data-Driven Method. *IEEE Trans. Power Electron.* **2026**, *41*, 11322–11336. https://doi.org/10.1109/tpel.2026.3658927.
63. Gómez, P.I.; Gajardo, M.E.L.; Mijatovic, N.; et al. A Self-Commissioning Edge Computing Method for Data-Driven Anomaly Detection in Power Electronic Systems. *IEEE Trans. Ind. Electron.* **2024**, *71*, 13319–13330. https://doi.org/10.1109/tie.2023.3347839.
64. Shen, X.; Zhang, X.; Shen, H.; et al. Identification of IGBT Bonding Wire Degradation Based on Feature Extraction and State Classification. *IEEE Trans. Power Electron.* **2025**, *40*, 15371–15380. https://doi.org/10.1109/tpel.2025.3577295.
65. Peng, Y.; Zhao, S.; Wang, H. A Digital Twin Based Estimation Method for Health Indicators of DC–DC Converters. *IEEE Trans. Power Electron.* **2021**, *36*, 2105–2118. https://doi.org/10.1109/tpel.2020.3009600.
66. Milton, M.; De La O, C.; Ginn, H.L.; et al. Controller-Embeddable Probabilistic Real-Time Digital Twins for Power Electronic Converter Diagnostics. *IEEE Trans. Power Electron.* **2020**, *35*, 9850–9864. https://doi.org/10.1109/tpel.2020.2971775.
67. Wang, S.; Ma, R. An Embedded Digital Twin of DC–DC based on Hybrid RLS for Real-Time Condition Monitoring. *IEEE J. Emerg. Sel. Top. Power Electron.* **2026**. https://doi.org/10.1109/jestpe.2026.3710051.
68. Peng, Y.; Wang, H. A Simplified On-State Voltage Measurement Circuit for Power Semiconductor Devices. *IEEE Trans. Power Electron.* **2021**, *36*, 10993–10997. https://doi.org/10.1109/tpel.2021.3070698.
69. Gill, L.; Rodriguez, L.A.G.; Kaplar, R.; et al. Novel On-State Voltage Measurement Circuit Topology, Operation, and Performance for High-Voltage Wide-Bandgap Devices. *IEEE Trans. Power Electron.* **2025**, *40*, 15433–15449. https://doi.org/10.1109/tpel.2025.3583677.
70. Liu, J.; Wei, X.; Yao, B.; et al. Integrated Short-Circuit Protection Method in On-State Voltage Measurement Circuit for SiC MOSFETs. *IEEE Trans. Power Electron.* **2026**, *41*, 7830–7846. https://doi.org/10.1109/tpel.2025.3643142.
71. Wu, Y.; Du, X. A VEN Condition Monitoring Method of DC-Link Capacitors for Power Converters. *IEEE Trans. Ind. Electron.* **2019**, *66*, 1296–1306. https://doi.org/10.1109/tie.2018.2835393.
72. Wang, H.; Xu, Z.; Ge, X.; et al. A Junction Temperature Monitoring Method for IGBT Modules Based on Turn-Off Voltage with Convolutional Neural Networks. *IEEE Trans. Power Electron.* **2023**, *38*, 10313–10328. https://doi.org/10.1109/tpel.2023.3278675.
73. McGrew, T.; Sysoeva, V.; Cheng, C.H.; et al. Condition Monitoring of DC-Link Capacitors Using Time–Frequency Analysis and Machine Learning Classification of Conducted EMI. *IEEE Trans. Power Electron.* **2022**, *37*, 12606–12618. https://doi.org/10.1109/tpel.2021.3135873.
74. Van Der Broeck, C.H.; Polom, T.A.; De Doncker, R.W. Degradation Diagnosis of Power Modules Based on Thermal Phase Response Sensing and Artificial Neural Networks. *IEEE Trans. Ind. Appl.* **2024**, *60*, 3438–3448. https://doi.org/10.1109/tia.2023.3334704.
75. Du, X.; Yang, Y.; Lv, J.; et al. Physics-Guided Deep Learning for Online Bond Wire Lift-Off Monitoring in IGBTs via Acoustic Emission. *IEEE Trans. Ind. Electron.* **2026**. https://doi.org/10.1109/tie.2026.3672753.
76. Zhu, M.; Liu, Y.; Huang, M.; et al. A Digital Twin System of Capacitive DC Bank Using Rogowski Coil to Monitor Individual Capacitors. *IEEE Trans. Power Electron.* **2023**, *38*, 9251–9260. https://doi.org/10.1109/tpel.2023.3271848.
77. Texas Instruments. UCC5870-Q1 30-A isolated IGBT/SiC MOSFET gate driver with advanced protection features for automotive applications. Datasheet SLUSD86C, October 2019, Revised September 2021. Available online: https://www.ti.com/lit/ds/symlink/ucc5870-q1.pdf (accessed on 7 October 2026).
78. Aichriedler, L.; Wriessnegger, G. Gate Charge and Leakage Measurement Test Sequence for Solid State Devices. U.S. Patent 12,306,240 B2, 20 May 2025.
79. *ISO 26262-5:2018*; Road Vehicles—Functional Safety—Part 5: Product Development at the Hardware Level; ISO: Geneva, Switzerland, 2018.
80. Wei, X.; Yao, B.; Wang, Z.; et al. A Robust Online Junction Temperature Calibration Method for Power Semiconductors in Traction Inverter Application. *IEEE Trans. Transp. Electrif.* **2025**, *11*, 6602–6614. https://doi.org/10.1109/tte.2024.3512941.
81. Peng, Y.; Shen, Y.; Wang, H. A Converter-Level On-State Voltage Measurement Method for Power Semiconductor Devices. *IEEE Trans. Power Electron.* **2021**, *36*, 1220–1224. https://doi.org/10.1109/tpel.2020.3009934.
82. Peng, Y.; Wang, H. A Self-Power Method for a Converter-Level On-State Voltage Measurement Concept. *IEEE Trans. Power Electron.* **2021**, *36*, 8743–8751. https://doi.org/10.1109/tpel.2021.3053202.

83. *AQG 324*; Qualification of Power Modules for Use in Power Electronics Converter Units in Motor Vehicles. ECPE: Nürnberg, Germany, 2025.
84. Zhang, Y.; Zhang, Y.; Wang, H. gEOL: A Gradient-Based End-of-Life Criterion for Power Semiconductor Modules. *IEEE Trans. Power Electron.* **2024**, *39*, 2927–2931. https://doi.org/10.1109/tpel.2023.3339342.
85. Saxena, A.; Celaya, J.; Saha, B.; et al. Metrics for Offline Evaluation of Prognostic Performance. *Int. J. Progn. Health Manag.* **2010**, *1*, 4–23. https://doi.org/10.36001/ijphm.2010.v1i1.1336.
86. Gao, J.; Chen, S.; Wang, D.; et al. Adaptive Remaining Useful Life Prediction for Film Capacitors in DC-Link Applications Using Degradation and Failure Data. *IEEE Trans. Power Electron.* **2026**, *41*, 5670–5683. https://doi.org/10.1109/tpel.2025.3621772.
87. Jiang, X.; Fan, T.; Qiu, Z.; et al. Lifetime Prediction of High-Current IGBT Modules Considering Bond Wire Degradation Under Nonconstant Stress. *IEEE J. Emerg. Sel. Top. Power Electron.* **2026**, *14*, 294–308. https://doi.org/10.1109/jestpe.2025.3585655.
88. Leppänen, J.A.R.; Hoffrén, A.L.J.; Leppänen, T.F.V.; et al. Early Detection of Wire Bond Degradation in IGBT Modules Using On-Chip Junction Temperature Sensor. *IEEE Trans. Power Electron.* **2026**, *41*, 5684–5697. https://doi.org/10.1109/tpel.2025.3621900.
89. Murdock, D.A.; Torres, J.E.R.; Connors, J.J.; et al. Active thermal control of power electronic modules. *IEEE Trans. Ind. Appl.* **2006**, *42*, 552–558. https://doi.org/10.1109/tia.2005.863905.
90. Andresen, M.; Ma, K.; Buticchi, G.; et al. Junction Temperature Control for More Reliable Power Electronics. *IEEE Trans. Power Electron.* **2018**, *33*, 765–776. https://doi.org/10.1109/tpel.2017.2665697.
91. Sangwongwanich, A.; Yang, Y.; Sera, D.; et al. Mission Profile-Oriented Control for Reliability and Lifetime of Photovoltaic Inverters. *IEEE Trans. Ind. Appl.* **2020**, *56*, 601–610. https://doi.org/10.1109/tia.2019.2947227.
92. Vernica, I.; Ma, K.; Blaabjerg, F. Optimal Derating Strategy of Power Electronics Converter for Maximum Wind Energy Production with Lifetime Information of Power Devices. *IEEE J. Emerg. Sel. Top. Power Electron.* **2018**, *6*, 267–276. https://doi.org/10.1109/jestpe.2017.2745714.
93. Ibrahim, A.; Salem, M.; Kamarol, M.; et al. Review of Active Thermal Control for Power Electronics: Potentials, Limitations, and Future Trends. *IEEE Open J. Power Electron.* **2024**, *5*, 414–435. https://doi.org/10.1109/ojpel.2024.3376086.
94. Andresen, M.; Buticchi, G.; Liserre, M. Study of reliability-efficiency tradeoff of active thermal control for power electronic systems. *Microelectron. Reliab.* **2016**, *58*, 119–125. https://doi.org/10.1016/j.microrel.2015.12.017.
95. Luo, H.; Iannuzzo, F.; Diaz Reigosa, P.; et al. Modern IGBT gate driving methods for enhancing reliability of high-power converters—An overview. *Microelectron. Reliab.* **2016**, *58*, 141–150. https://doi.org/10.1016/j.microrel.2015.12.022.
96. Ko, Y.; Andresen, M.; Buticchi, G.; et al. Discontinuous-Modulation-Based Active Thermal Control of Power Electronic Modules in Wind Farms. *IEEE Trans. Power Electron.* **2019**, *34*, 301–310. https://doi.org/10.1109/tpel.2018.2819423.
97. Liserre, M.; Andresen, M.; Costa, L.; et al. Power Routing in Modular Smart Transformers: Active Thermal Control Through Uneven Loading of Cells. *IEEE Ind. Electron. Mag.* **2016**, *10*, 43–53. https://doi.org/10.1109/mie.2016.2588898.
98. Konstantinou, G.; Pou, J.; Ceballos, S.; et al. Active Redundant Submodule Configuration in Modular Multilevel Converters. *IEEE Trans. Power Deliv.* **2013**, *28*, 2333–2341. https://doi.org/10.1109/tpwrd.2013.2264950.
99. Peyghami, S.; Palensky, P.; Fotuhi-Firuzabad, M.; et al. System-Level Design for Reliability and Maintenance Scheduling in Modern Power Electronic-Based Power Systems. *IEEE Open Access J. Power Energy* **2020**, *7*, 414–429. https://doi.org/10.1109/oajpe.2020.3029229.
100. Ma, K.; Liserre, M.; Blaabjerg, F. Reactive Power Influence on the Thermal Cycling of Multi-MW Wind Power Inverter. *IEEE Trans. Ind. Appl.* **2013**, *49*, 922–930. https://doi.org/10.1109/tia.2013.2240644.
101. Semikron Danfoss. Cosmic Ray Failures in Power Electronics. Application Note AN 17-003. 2024. Available online: https://assets.danfoss.com/documents/latest/465381/AB501641368473en-000201.pdf (accessed on 7 October 2026).
102. Andresen, M.; Raveendran, V.; Buticchi, G.; et al. Lifetime-Based Power Routing in Parallel Converters for Smart Transformer Application. *IEEE Trans. Ind. Electron.* **2018**, *65*, 1675–1684. https://doi.org/10.1109/tie.2017.2733426.
103. Alcaide, A.M.; Guenter, S.; Leon, J.I.; et al. Integral Hierarchical Degradation Management-Oriented Control of Parallel-Connected DC/DC Converters. *IEEE Trans. Ind. Electron.* **2026**. https://doi.org/10.1109/tie.2026.3672741.
104. Lee, G.; Chae, S. Active Thermal Balancing Strategy for DAB Converter Based on On-State Resistance Imbalance Estimation Among MOSFETs. *IEEE Open J. Power Electron.* **2026**, *7*, 2301–2313. https://doi.org/10.1109/ojpel.2026.3717772.
105. Zhang, J.; Du, X.; Qian, C.; et al. Thermal Management of IGBT Module in the Wind Power Converter Based on the ROI. *IEEE Trans. Ind. Electron.* **2022**, *69*, 8513–8523. https://doi.org/10.1109/tie.2021.3108729.